











A fundamental plane of black hole accretion at millimetre wavelengths

Ilaria Ruffa ^{1,2*}, Timothy A. Davis ¹, Jacob S. Elford ^{1,†}, Martin Bureau,³ Michele Cappellari ³,
Jindra Gensior ⁴, Daryl Haggard,⁵ Satoru Iguchi ^{6,7}, Federico Lelli ⁸, Fu-Heng Liang,³ Lijie Liu ^{9,10},
Marc Sarzi,¹¹ Thomas G. Williams ³ and Hengyue Zhang ³

¹Cardiff Hub for Astrophysics Research & Technology, School of Physics & Astronomy, Cardiff University, Queens Buildings, The Parade, Cardiff CF24 3AA, UK

²INAF – Istituto di Radioastronomia, via P. Gobetti 101, I-40129 Bologna, Italy

³Sub-department of Astrophysics, Department of Physics, University of Oxford, Keble Road, Oxford OX1 3RH, UK

⁴Institute for Computational Science, University of Zurich, Winterthurerstrasse 190, CH-8057 Zurich, Switzerland

⁵Trottier Space Institute and Department of Physics, McGill University, 3600 Rue University, Montreal QC H3A 2T8, Canada

⁶Department of Astronomical Science, SOKENDAI (The Graduate University of Advanced Studies), Mitaka, 181-8588 Tokyo, Japan

⁷National Astronomical Observatory of Japan, National Institutes of Natural Sciences, Mitaka, Tokyo 181-8588, Japan

⁸INAF, Arcetri Astrophysical Observatory, Largo Enrico Fermi 5, I-50125 Florence, Italy

⁹Cosmic Dawn Center (DAWN), Technical University of Denmark, DK-2800 Kgs. Lyngby, Denmark

¹⁰DTU-Space, Technical University of Denmark, Elektrovej 327, DK-2800 Kgs. Lyngby, Denmark

¹¹Armagh Observatory and Planetarium, College Hill, Armagh BT61 9DG, UK

Accepted 2023 November 1. Received 2023 November 1; in original form 2023 July 26

ABSTRACT

We report the discovery of the ‘mm fundamental plane of black hole accretion’, which is a tight correlation between the nuclear 1 mm luminosity ($L_{\nu, \text{mm}}$), the intrinsic 2–10 keV X-ray luminosity ($L_{X, 2-10}$) and the supermassive black hole (SMBH) mass (M_{BH}) with an intrinsic scatter (σ_{int}) of 0.40 dex. The plane is found for a sample of 48 nearby galaxies, most of which are low-luminosity active galactic nuclei. Combining these sources with a sample of high-luminosity (quasar-like) nearby AGN, we show that the plane still holds. We also find that M_{BH} correlates with $L_{\nu, \text{mm}}$ at a highly significant level, although such correlation is less tight than the mm fundamental plane ($\sigma_{\text{int}} = 0.51$ dex). Crucially, we show that spectral energy distribution (SED) models for both advection-dominated accretion flows (ADAFs) and compact jets can explain the existence of these relations, which are not reproduced by the standard torus-thin accretion disc models usually associated to quasar-like AGN. The ADAF models reproduces the observed relations somewhat better than those for compact jets, although neither provides a perfect fit. Our findings thus suggest that radiatively inefficient accretion processes such as those in ADAFs or compact (and thus possibly young) jets may play a key role in both low- and high-luminosity AGN. This mm fundamental plane also offers a new, rapid method to (indirectly) estimate SMBH masses.

Key words: black hole physics – galaxies: active – galaxies: nuclei – submillimetre: galaxies – X-rays: galaxies.

1 INTRODUCTION

The many details of the processes regulating the connection between the growth of central supermassive black holes (SMBHs) and the evolution of their host galaxies (so-called ‘co-evolution’; e.g. Kormendy & Ho 2013) are still poorly understood (e.g. D’Onofrio, Marziani & Chiosi 2021). Understanding the physics of accretion on to SMBHs, determining if and how it changes in objects with different types of nuclear activity, as well as setting accurate constraints on fundamental SMBH properties such as its mass, are all crucial steps to get a comprehensive view of the SMBH–host galaxy interplay.

The so-called ‘fundamental plane of BH accretion’ (hereafter FP) is an empirical correlation between the SMBH masses (M_{BH}),

5 GHz radio ($L_{5\text{GHz}}$), and 2–10 keV X-ray ($L_{X, 2-10}$) luminosities, which was initially reported by Merloni, Heinz & di Matteo (2003) and Falcke, Körding & Markoff (2004). The origin of the FP is still debated, but it is widely believed to carry information on the physics of SMBH accretion (see e.g. Gültekin et al. 2019a). However, the scatter around this correlation varies significantly depending on the sample and the method used to fit the plane, reaching values up to 0.88 dex (e.g. Merloni, Heinz & di Matteo 2003; Gültekin et al. 2009, 2019a; Plotkin et al. 2012; Saikia, Körding & Falcke 2015, and references therein). Furthermore, the nature of the radio emission in the FP is not yet well-understood (potentially arising from compact jets or complex shock dynamics). All the above somehow limit the diagnostic power of the FP.

In this Letter, we report the discovery of an FP at millimetre wavelengths, namely the existence of a tight correlation between the nuclear (i.e. $\ll 100$ pc) mm luminosities ($L_{\nu, \text{mm}}$), M_{BH} , and intrinsic $L_{X, 2-10}$, which we find to hold for both high- and low-luminosity

* E-mail: ruffai@cardiff.ac.uk

† First-authorship is shared between Ruffa, Davis, and Elford

AGN (within $z \lesssim 0.05$). We also present the analysis of the physics underlying such correlation, and discuss how our results may have profound implications for our understanding of BH accretion in different AGN types.

2 PRIMARY SAMPLE AND DATA

Our sample was primarily drawn from the mm-Wave Interferometric Survey of Dark Object Masses (WISDOM) project, which mainly exploits high-resolution Atacama Large Millimeter/submillimeter Array (ALMA) CO observations to dynamically estimate SMBH masses in a varied sample of galaxies (e.g. Davis et al. 2017). We included 31 WISDOM galaxies (see online material) at $z \lesssim 0.03$, spanning a range of AGN bolometric luminosities ($L_{\text{bol}} = 10^{41} - 10^{46}$ erg s $^{-1}$) and mostly (but not exclusively) having very low rates of accretion onto their central SMBHs ($\dot{M} \lesssim 10^{-3} M_{\text{Edd}}$; Elford et al. 2023). As such, most of these objects are classified as low-luminosity AGN (LLAGN; Ho 2008). To increase the statistics, we supplemented these 31 with a further 17 galaxies (see online material), selected from the literature to have dynamical SMBH masses, existing high-resolution ALMA 1 mm and high-quality X-ray data. The majority of these are nearby ellipticals and span ranges of L_{bol} and \dot{M} similar to those of the WISDOM sources. Hereafter, we refer to the 31 WISDOM plus 17 literature sources as the *primary sample*.

The 1 mm luminosities of the primary sample sources were derived from high-angular-resolution ALMA Band 6 continuum observations, taken between 2013 and 2021 as part of a large number of projects (see online material). All data were reduced using the Common Astronomy Software Applications (CASA) pipeline (McMullin et al. 2007), adopting a version appropriate for each data set and a standard calibration strategy. For more details on the data reduction see Davis et al. (2022).

For each data set, continuum images were produced by combining the continuum spectral windows (SPWs) and the line-free channels of the line SPW (when included) using the CASA task TCLEAN in multifrequency synthesis (MFS) mode. The resulting continuum maps have synthesised beams ranging from 0."042 to 0."723, corresponding to 6–330 pc (average spatial resolution ≈ 25 pc). For each source, we measured the continuum flux density f_{mm} from the innermost synthesised beam, coincident with the galaxy core. The mm luminosities were then estimated as $L_{\nu, \text{mm}} = 4\pi D_L^2 f_{\text{mm}} \nu_{\text{obs}}$, where D_L is the luminosity distance and ν_{obs} the observed frequency (between 231 and 239 GHz). As all the data were obtained with long-baseline configurations, extended dust emission is resolved out. We indeed typically detect only a point-like source at each galaxy centre, arising from unresolved core emission. In three (out of 48) galaxies, the emission is slightly resolved, making our measurements more uncertain. Removing these three objects, however, does not affect our results in any way. The obtained $L_{\nu, \text{mm}}$ are listed in Table 1 of online material.

The intrinsic (absorption-corrected) 2–10 keV luminosities ($L_{\text{X}, 2-10}$) of the primary sample sources were retrieved from the literature, as detailed in Elford et al. (2023). In short, eight of these galaxies have no X-ray data available and were thus not considered in the parts of the analysis where $L_{\text{X}, 2-10}$ was required. For the vast majority of the objects with X-ray data (33/40), the adopted $L_{\text{X}, 2-10}$ was derived from *Chandra* observations, including only emission from the unresolved AGN core. For most of the *Chandra*-observed objects (26/33), accurate (intrinsic) nuclear $L_{\text{X}, 2-10}$ were retrieved from the catalogue of Bi, Feng & Ho (2020, see also online material).

Dynamically determined SMBH masses (from stellar, ionized gas, molecular gas, and/or maser kinematics) are available for a total of 31 primary sample sources (see online material). For the remaining 17 galaxies, we estimated M_{BH} using the $M_{\text{BH}} - \sigma_*$ relation of van den Bosch (2016), where σ_* is the stellar velocity dispersion within one effective radius. This was retrieved from the compilations of van den Bosch (2016) and Cappellari et al. (2013) when available, from the HyperLeda data base otherwise (<http://leda.univ-lyon1.fr>). Crucially, although constructed based on data availability only (and thus not meant to be complete in any statistical sense), our primary sample spans four orders of magnitude in SMBH mass.

3 THE MM FUNDAMENTAL PLANE

As illustrated in Fig. 1 (left panel), the SMBH masses of our primary sample galaxies strongly correlate with their $L_{\nu, \text{mm}}$. A power law was fitted to the observed trend, using the LTS_LINEFIT routine (Cappellari et al. 2013). This combines the least-trimmed-squares (LTS) robust regression technique (Rousseeuw 1984) with a least-squares fitting algorithm, and allows for intrinsic scatter and uncertainties in all coordinates. The resulting best-fitting power law is

$$\log_{10} \left(\frac{M_{\text{BH}}}{M_{\odot}} \right) = (0.79 \pm 0.08) \left[\log_{10} \left(\frac{L_{\nu, \text{mm}}}{\text{erg s}^{-1}} \right) - 39 \right] + (8.2 \pm 0.1), \quad (1)$$

with an observed scatter (σ_{obs}) of 0.55 dex and an estimated intrinsic scatter (σ_{int}) of 0.51 ± 0.08 dex. When including $L_{\text{X}, 2-10}$, we discover the existence of a tighter correlation (Fig. 1, right panel). In this case, we used the LTS_PLANEFIT routine (Cappellari et al. 2013) to find the best-fitting plane in the $(\log M_{\text{BH}}, \log L_{\text{X}, 2-10}, \log L_{\nu, \text{mm}})$ space

$$\log_{10} \left(\frac{M_{\text{BH}}}{M_{\odot}} \right) = (-0.23 \pm 0.05) \left[\log_{10} \left(\frac{L_{\text{X}, 2-10}}{\text{erg s}^{-1}} \right) - 40 \right] + (0.95 \pm 0.07) \left[\log_{10} \left(\frac{L_{\nu, \text{mm}}}{\text{erg s}^{-1}} \right) - 39 \right] + (8.35 \pm 0.08), \quad (2)$$

with $\sigma_{\text{obs}} = 0.45$ dex and $\sigma_{\text{int}} = 0.40 \pm 0.07$ dex. We verified that this multivariate plane fit provides a significantly better predictor for M_{BH} than the simple line fit, having a $\Delta_{\text{BIC}} \gg 10$ (where Δ_{BIC} is the difference in the Bayesian information criterion between the line and plane fits). For both correlations, we also performed Spearman rank analyses to quantify their statistical significance, and show the resulting correlation coefficients in the top left corner of each panel of Fig. 1. Since the nuclear mm and X-ray emission from AGN is known to be time variable (typically by a factor of 2–3 over year time-scales; Prieto et al. 2016; Fernández-Ontiveros et al. 2019; Behar et al. 2020), variability likely dominates the observed scatters (and thus the underlying correlations may be tighter). By analogy with the previous FP, we dub the correlation in the right panel of Fig. 1 as the ‘mm fundamental plane of BH accretion’ (hereafter mmFP).

We note that the error budget of the derived $L_{\nu, \text{mm}}$ is dominated by the ALMA flux calibration uncertainties ($\approx 10\%$ for Band 6 data). These are, however, much smaller than the estimated intrinsic scatters of the correlations in Fig. 1 (see above), and thus have a negligible impact on our results. We also note that the $L_{\text{X}, 2-10}$ of the five X-ray observed sources without available *Chandra* data could be slightly overestimated, due to contamination from diffuse hot gas in the galactic and circumgalactic medium (CGM; although this mainly emits in the 0.3–2 keV range) and/or X-ray binaries. While we verified that any such contamination should be minimal (based on the

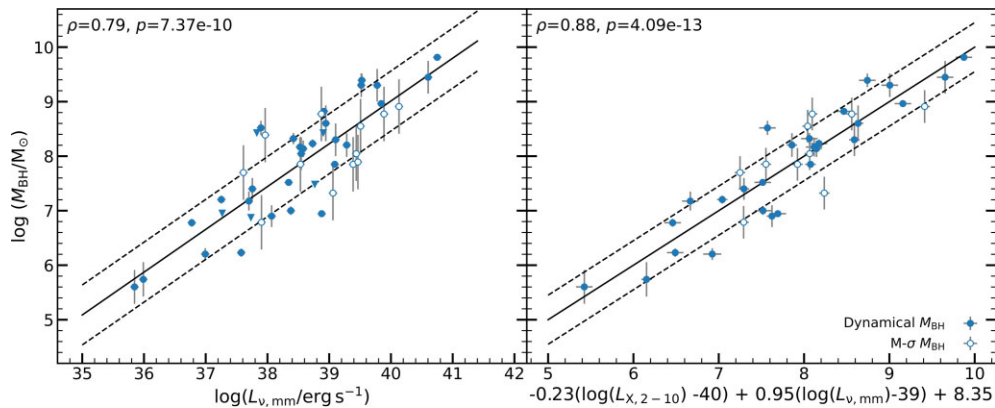


Figure 1. Correlation between M_{BH} and $L_{\nu, \text{mm}}$ (left panel) and edge-on view of the $M_{\text{BH}}-L_{X, 2-10}-L_{\nu, \text{mm}}$ correlation (right panel) for the primary sample galaxies. In both panels, filled blue circles show sources with dynamical M_{BH} measurements, open circles sources with M_{BH} from the $M_{\text{BH}}-\sigma_*$ relation of van den Bosch (2016). Error bars are plotted for all points but some are smaller than the symbol used. The best-fitting power laws are overlaid as a black solid line, the observed scatter as black dashed lines. The correlation coefficients ρ and p -values of the performed Spearman rank analysis are reported in the top left corner of each panel.

scaling laws of Grimm, Gilfanov & Sunyaev 2003, Kim & Fabbiano 2004, and Boroson, Kim & Fabbiano 2011), we cannot rule it out entirely. In any case, removing these five sources does not make any relevant change in the best-fitting parameters of the mmFP. The same applies when removing the sources without a robust, dynamical M_{BH} estimate (the best-fitting line and planes are identical, within their respective errors, and the observed scatters become only slightly smaller).

3.1 BASS galaxies

Although the majority of the primary sample galaxies are LLAGN, a handful are more luminous systems (see Elford et al. 2023), which still follow the mmFP. To investigate whether this result holds more generally, we built a comparison sample from the *Swift*-BAT AGN Spectroscopic Survey (BASS), comprising AGN with median $z = 0.05$, $L_{\text{bol}} = 10^{44} \text{ erg s}^{-1}$, and $M = 0.01 - 0.1 \dot{M}_{\text{Edd}}$ (Koss et al. 2017). We included only the BASS sources for which both ALMA 1 mm observations (with spatial resolutions similar to those of the primary sample) and nuclear intrinsic $L_{X, 2-10}$ were available (88 sources; Kawamuro et al. 2022). The SMBH masses of these objects were taken from the compilation of Koss et al. (2022). The BASS galaxies are typically more distant than those in the primary sample, so their M_{BH} have been estimated with a variety of methods (see Fig. 2). However, most of the sources (50/88) have their M_{BH} from the $M_{\text{BH}}-\sigma_*$ relation of Kormendy & Ho (2013). We recalibrated these measurements using the $M_{\text{BH}}-\sigma_*$ relation of van den Bosch (2016), for consistency with the 17 primary sample sources without a dynamical SMBH mass estimate.

As illustrated in Fig. 3(b), the BASS sources are in agreement with the best-fitting mmFP, albeit with a larger observed scatter. We performed a Spearman rank analysis to quantify the statistical significance of this relation for the BASS points alone, and verified that they do show a significant correlation ($p = 0.002$), but with a correlation coefficient ($\rho = 0.32$) smaller than that of the primary sample. Fig. 2 suggests that the larger scatter in this population is (at least partly) driven by the M_{BH} uncertainties, as the position of a BASS galaxy with respect to the best-fitting mmFP depends on the method used to estimate its M_{BH} . For instance, sources with M_{BH} from reverberation mapping or broad-line methods are located systematically below the best-fitting line, likely reflecting

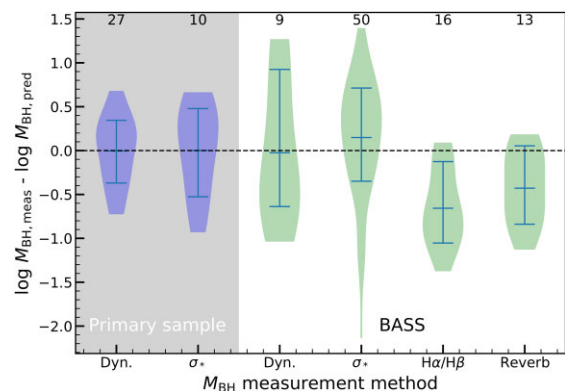


Figure 2. Residuals of our primary sample (grey shaded region) and BASS sources (white region) from the best-fitting mmFP, plotted as a function of the SMBH mass measurement method. ‘Dyn’ refers to dynamical mass measurements, ‘ σ_* ’ to estimates from the $M_{\text{BH}}-\sigma_*$ relation of van den Bosch (2016), ‘ $\text{H}\alpha/\text{H}\beta$ ’ to the broad-line method and ‘Reverb’ to reverberation mapping. Each set of data points is represented by a violin describing the underlying distribution. The number of sources in the mmFP whose M_{BH} has been estimated using that particular method is indicated above each violin. In each case, the blue horizontal lines denote the 18th, 50th, and 85th percentiles of the distribution.

the different biases in place when using such techniques (e.g. Farrah et al. 2023).

4 PHYSICAL DRIVERS

The fact that the BASS galaxies are consistent with a relation primarily defined by LLAGN is surprising. To determine the underlying physics, we compared the observed nuclear mm and X-ray luminosities of both the primary sample and BASS sources to those extracted from mock nuclear SEDs arising from both ‘classic’ and radiatively-inefficient (ADAF-like) accretion flows, and from compact radio jets.

4.1 Torus model

AGN in the BASS sample (and a few in the primary sample) have *estimated* accretion rates in the range $\dot{M} \sim 0.01 - 0.1 \dot{M}_{\text{Edd}}$. Accord-

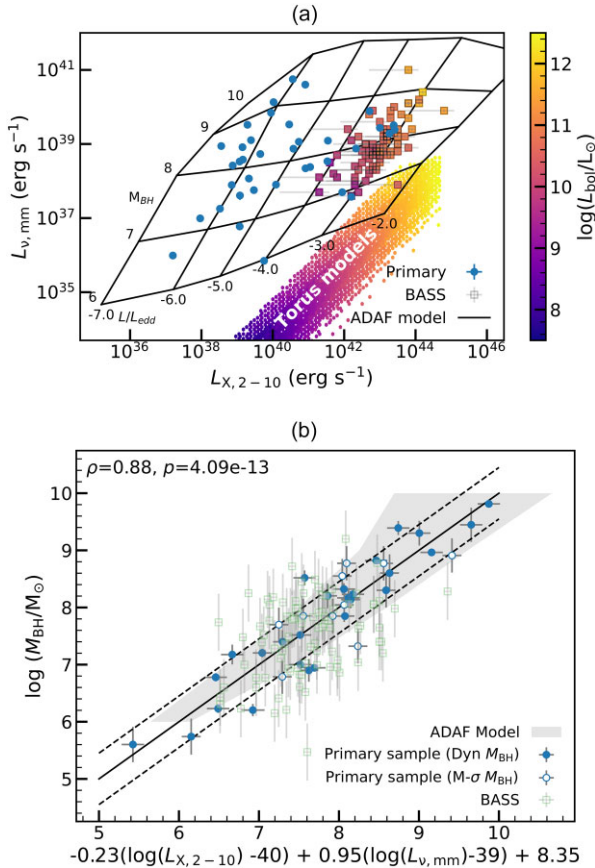


Figure 3. (a): Correlation between $L_{X, 2-10}$ and $L_{\nu, \text{mm}}$ for the primary sample (blue circles) and the BASS (square symbols, coloured by their L_{bol}) sources. Error bars are plotted for all points but some are smaller than the symbol used. The black grid illustrates the area covered by the ADAF model solutions as a function of M_{BH} and the Eddington ratio L/L_{Edd} (Section 4.2). The purple–yellow coloured bins indicate the region covered by the extrapolated SKIRTOR torus models (Section 4.1), where each hexagonal bin is coloured by the mean L_{bol} of the sources within that bin. (b): As the right panel of Fig. 1, but with the BASS galaxies overlaid as green squares and the grid of ADAF models from Fig. 3 (a) projected onto the plane as a grey shaded area (including a small offset for clarity; see Section 4.2).

ing to the standard paradigm, in this type of systems the accretion should occur through the classic geometrically-thin and optically-thick accretion disc surrounded by a dusty torus (e.g. Heckman & Best 2014). In this scenario, both the mm and the 2–10 keV emission are expected to arise from the accretion disc, reprocessed by dust in the torus in the mm and Compton-up scattered by the hot corona in X-rays. To check if this type of model can reproduce the observed mm and X-ray luminosities, we used the SKIRTOR library (Stalevski et al. 2012, 2016). The SED models were retrieved from the SKIRTOR webpage (<https://sites.google.com/site/skirtorus/>), but their spectral coverage (from 300 GHz to 1.24 keV) is slightly shorter than that required for this work. We thus expanded the models to the full range of wavelengths probed here, treating the emission mechanisms self-consistently as prescribed in the original version of the code (i.e. using the same grey-body curve for millimetre emission, and a power law in the X-ray regime; Yang et al. 2020). We followed the prescriptions of Stalevski et al. (2012, 2016) to scale the models for different L_{bol} , in the range $10^{7.5} - 10^{12.5} L_{\odot}$ (i.e. the range covered by the primary and BASS sources; the torus is expected to disappear at low accretion rates, but the resulting model predictions are neverthe-

less instructive). For each SKIRTOR SED model, we then extracted the predicted 1 mm (specifically, the luminosity at 237.5 GHz, that is the median ALMA continuum frequency for both the primary and BASS sources) and intrinsic 2–10 keV luminosities, and compared them with the measured ones. The resulting predictions are shown in Fig. 3(a) as a hexagonally binned histogram (coloured by mean L_{bol}). The luminosities extracted from the torus models reasonably reproduces the slope of the $L_{X, 2-10} - L_{\nu, \text{mm}}$ relation of the BASS sources, but with an offset of about two orders of magnitude at a given L_{bol} . On the other hand, to explain $L_{\nu, \text{mm}}$ of the lower accretion rate galaxies, the mm luminosities in the SKIRTOR models would need to be at least four orders of magnitude larger at a given accretion rate (and thus X-ray luminosity).

4.2 ADAF model

To build model SEDs arising from radiatively-inefficient accretion flows around SMBHs, we used the ‘LLAGN’ model of Pesce et al. (2021, itself a development of previous models by Narayan & Yi 1995a; Mahadevan 1997). In typical LLAGN and some (low-accretion rate) Seyferts, the classic accretion disc is either absent or truncated at some inner radius (the transition usually happens beyond a few tens of Schwarzschild radii), and replaced by a geometrically-thick two-temperature structure in which the ion temperature is greater than the electron temperature and the accretion occurs at rates well below the Eddington limit (i.e. $\ll 0.01 \dot{M}_{\text{Edd}}$; Narayan & Yi 1995b; Ho 2008). The electrons in such radiatively-inefficient flows (such as advection-dominated accretion flows; ADAFs) cool down via a combination of self-absorbed synchrotron, bremsstrahlung, and inverse Compton radiation, which together give rise to the nuclear SED from the mm to the X-rays. The LLAGN model adopted here solves for the energy balance between the heating and cooling of the electrons in the flow. We generated a set of model SEDs for a grid of SMBH masses ($10^6 - 10^{10} M_{\odot}$) and Eddington ratios ($10^{-7} - 10^{-2}$), while all the other free parameters were kept at the defaults discussed in appendix A of Pesce et al. (2021). We then extracted the predicted 237.5 GHz and 2–10 keV luminosities, as described above. As illustrated by the shape of the model grid in Fig. 3(a), the mm and X-ray luminosities of all the sources (and thus the observed correlations) are well explained if they arise from an ADAF-like accretion mechanism. The grid is almost aligned with the axes, thus predicting that the mm luminosity primarily depends on M_{BH} , while $L_{X, 2-10}$ primarily traces the Eddington ratio. The tighter correlation obtained when including $L_{X, 2-10}$ can be explained by the fact that the slight tilt of the grid is then taken into account, especially at higher Eddington ratios. A 3D version of Fig. 3(a) (including all the primary sample and only the BASS sources with the most robust, dynamical M_{BH} measurements; see Section 3.1 and Fig. 2) is provided as supplementary online material. In Fig. 3(b), we show the projection of the ADAF model grid on to the best-fitting mmFP. This latter seems to arise naturally from these models, as an (almost) edge-on view of the 3D $M_{\text{BH}} - L_{X, 2-10} - L_{\nu, \text{mm}}$ relation. We note, however, that keeping the default model parameters from Pesce et al. (2021), the model well predicts the gradient of the mmFP, but is offset by a small amount (i.e. the model overpredicts $L_{\nu, \text{mm}}$ at a given SMBH mass by ≈ 0.5 dex). Tweaking the model parameters to reduce the effective radiative efficiency easily removes this offset (e.g. by changing some combination of the effective viscosity, ratio of gas to magnetic pressure, fraction of viscous heating going directly to the electrons, outer radius of the ADAF, and/or power-law index of the mass accretion rate as a function of radius). However, as the correct values of these parameters are not well-constrained, here we

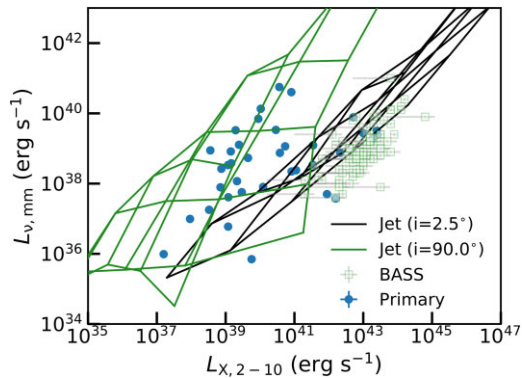


Figure 4. As Fig. 3, but with slightly expanded axis ranges. In this case, the grids overlaid in black and green illustrate the areas covered by the compact jet model solutions as a function of M_{BH} and the jet power, for jet inclinations of 2.5° and 90° , respectively. Solutions with intermediate inclinations lie in-between these two extremes (see Section 4.3).

simply offset the model grid by a constant 0.5 dex in SMBH mass to align it with the observed correlation. We stress that this scaling factor is significantly smaller than the one required for torus models to reproduce the observed trend (see Section 4.1), and is well within the uncertainties for the adopted model parameters (see Pesce et al. 2021). Future work exploring the parameters of ADAF-like models in sources with more extensive (sub-)mm coverage will allow to better understand the observed correlation, the small offset, and the physics of accretion onto these SMBHs. This is discussed further in Section 5.

4.3 Compact jet model

Unlike extended jets (where the synchrotron emission is optically thin), compact radio jets have self-absorbed synchrotron spectra (similar to those from ADAFs) and have been argued to dominate the nuclear SEDs of LLAGN. In some cases, they are preferred over a pure ADAF solution, as this would be overly luminous at near-infrared and optical wavelengths (e.g. Fernández-Ontiveros, López-López & Prieto 2023). To determine if compact jets can explain the observed trends, we used the BHJET model of Lucchini et al. (2022). We fixed most of the model parameters to the values found for M81, a prototypical AGN with compact jets (Model B in table 3 of Lucchini et al. 2022), and generated a grid of models varying the SMBH mass (10^6 – $10^{10} M_\odot$), jet power ($10^{-5.5}$ – $10^{-0.5} L_{\text{Edd}}$) and jet inclination to the line of sight (2.5° – 90°). We then extracted from the resulting model SEDs the predicted $L_{\nu, \text{mm}}$ and $L_{X, 2-10}$ (as above), and compare them with the observed ones. In Fig. 4, we show the $L_{X, 2-10} - L_{\nu, \text{mm}}$ relation with overlaid the resulting model grids for the extremes in jet inclination (2.5° and 90°). Jets at intermediate inclinations lie between these two extremes (but evolve quickly towards the $i = 90^\circ$ solution once the line-of-sight is no longer aligned along the jet cone). The model grids encompass the majority of the LLAGN and some BASS sources, but they have significant curvature in the 3D $M_{\text{BH}} - L_{X, 2-10} - L_{\nu, \text{mm}}$ space (as for Fig. 3a, a 3D version of Fig. 4 is provided in the online material). The correlations in Fig. 1 do not seem to occur naturally within this model (as projections of the higher-order surface on to the axes). The luminosities of high-accretion-rate AGN from the primary and the BASS samples are harder to explain with these models, and would require additional X-ray emitting components. This is perhaps unsurprising, as compact jet models are substantially more complex than ADAFs (see also Section 5).

4.4 Distance uncertainties

Both M_{BH} and luminosity measurements are systematically affected by the assumed galaxy distance D , with $M_{\text{BH}} \propto D$ and $L \propto D^2$. Large distance errors can thus introduce large uncertainties on M_{BH} and L , and the difference in how these quantities scale with distance can give rise to spurious correlations. To test that this is not affecting our results, we performed a simple Monte Carlo simulation, drawing M_{BH} and the luminosities from independent Gaussian distributions that are truly uncorrelated, forcing a correlation to arise due to distance errors alone. The magnitude of the distance errors required to reproduce the Spearman rank correlation coefficients in Fig. 1 turned out to be ≥ 1.5 dex, much higher than that of our primary sample sources and – more in general – expected for real distance measurements. In addition, the slope of relations purely due to distance uncertainties would be substantially flatter than those observed (gradients of 0.5 for the $M_{\text{BH}} - L_{\nu, \text{mm}}$ correlation and 0.25 for the mmFP, as opposed to the observed ≈ 0.8 and ≈ 1 , respectively).

To further check for any systematic distance bias, we carried out a simple quality-checking exercise for our primary sample. We restricted our analysis to only those sources with the most accurate (redshift-independent) distances (26/48), i.e. derived from surface brightness fluctuations, tip of the red giant branch methods, supernovae, Cepheids, masers, the planetary nebula luminosity function, and the globular cluster luminosity function. This led us to obtain much tighter correlations, with an intrinsic scatter of 0.19 dex for the $M_{\text{BH}} - L_{\nu, \text{mm}}$ relation and only 0.11 dex for the mmFP. The corresponding Spearman rank coefficients are $\rho = 0.84$ ($p = 5.05 \times 10^{-7}$) and $\rho = 0.93$ ($p = 2.67 \times 10^{-9}$), respectively. We thus conclude that our results are not biased due to distance uncertainties.

5 DISCUSSION AND CONCLUSIONS

We report here the finding of tight $M_{\text{BH}} - L_{\nu, \text{mm}}$ and $M_{\text{BH}} - L_{X, 2-10} - L_{\nu, \text{mm}}$ correlations (Fig. 1). We dub the latter the ‘mm fundamental plane of BH accretion’ and find it to hold for both low- (mostly WISDOM) and high- (mostly BASS) luminosity AGN. To understand the physics underlying the mmFP, we compared the observed trend with models predicting the emission from different nuclear mechanisms. We find that the results for both our sample and the BASS sources are best explained if their emission in the mm and X-rays primarily arises from an ADAF-like process, but cannot be explained by a classic torus model (see Fig. 3). This suggests that some kind of radiatively inefficient accretion process may play a role in both low- and high-luminosity AGN, at least in the range of luminosities and accretion rates probed by the sources included in this work. While torii are known to exist in many of these AGNs, some regions around their SMBHs may be radiatively inefficient. For instance, some accretion disc solutions allow discs to transition from ADAF-like to geometrically-thin (and vice versa at different radii), and ADAFs could also exist above and below classic accretion discs (Mahadevan 1997). Although the exact conditions under which this applies are still to be investigated, it is clear that our results may have profound implications for our understanding of BH accretion in many different types of AGN.

We also explored the possibility that both the mm and X-ray emissions arise from compact (and thus probably young; O’Dea & Saikia 2020) radio jets (Section 4.3). These have been argued to dominate the whole SEDs of LLAGN (e.g. Fernández-Ontiveros, López-López & Prieto 2023) and have spectral properties similar to those of an ADAF at the wavelengths probed here. This is also consistent with one of the most popular scenarios for the origin

of the radio FP of LLAGN, suggesting that the correlation arises from strongly sub-Eddington jet-dominated emission (e.g. Falcke, Körding & Markoff 2004; Plotkin et al. 2012). The contribution of compact jets to the nuclear SEDs of radiatively-efficient, quasar-like AGN is instead still hotly debated (e.g. Fawcett et al. 2020; Girdhar et al. 2022). Our results are marginally consistent with these scenarios, as we find that compact jet models can explain the correlations for most of the LLAGN, but additional X-ray emitting components are required in the higher-luminosity systems.

In short, we demonstrated that ADAF-like models convincingly predict the mmFP. Compact jets are also a plausible explanation (at least for LLAGN), but the corresponding models do not reproduce the correlation as naturally as the ADAF-like ones. We caution, however, that the plasma physics underlying both the ADAF and compact jet models is not well-constrained, and significant uncertainties are present in all the model parameters and how they interact. We thus conclude that, while ‘classic’ torus models seem to be ruled out, either ADAF-like or compact jet emission have the potential to explain the observed trend. The presence of one (or more) of these mechanisms could even help explaining the increased far-infrared/sub-mm contribution attributed to AGN in some empirical SED models (e.g. Symeonidis 2022). The tight $L_{X, 2-10} - L_{v, mm}$ correlation observed in Fig. 3 a for the BASS sources is also consistent with the one reported by Ricci et al. (2023) between the 100 GHz and 14–150 keV luminosities (see also Behar et al. 2018), and our results add interesting clues onto its origin. Determining with certainty the relevant mechanism(s) giving rise to the observed correlations is beyond the scope of this work, but is crucial to further our understanding of the SMBH accretion/ejection processes in different AGN types.

Beyond carrying information on the nuclear physics, the correlations presented here provide new rapid methods to indirectly estimate the mass of SMBHs (or their accretion rates, if one has alternative, robust estimates of M_{BH} and $L_{v, mm}$; see e.g. Ricci et al. 2023). Although direct M_{BH} estimates can be obtained using a variety of techniques (e.g. stellar or gas kinematics, reverberation mapping), these typically require very time consuming observational campaigns and currently have limited application beyond the local Universe. The ability to use nuclear mm and (optionally) X-ray luminosities allows M_{BH} estimates when dynamical measurements are not possible and/or the standard scaling relations are unusable (such as in dwarf or disturbed galaxies). It also allows M_{BH} predictions over a wider range of redshifts. At the high-mass end of the correlations, ALMA can allow us to constrain M_{BH} up to $z \approx 0.3$ (and is limited more by angular resolution and frequency coverage than sensitivity). Proposed new interferometers (such as the next-generation Very Large Array, ngVLA) should be able to push this to $z = 1$ and beyond. Large X-ray surveys that can provide complementary X-ray data are also ongoing (e.g. eROSITA), and next-generation satellites (such as the *Advanced Telescope for High ENergy Astrophysics*, *Athena*) will extend these to higher- z . We also note that the intrinsic scatter of the $M_{BH} - L_{v, mm}$ relation is comparable to that of the $M_{BH} - \sigma_*$ relation (e.g. van den Bosch 2016), and σ_{int} of the mmFP in Fig. 1 is comparable or even lower than that of its radio counterpart (depending on the sample used to fit the plane; see e.g. Merloni, Heinz & di Matteo 2003; Falcke, Körding & Markoff 2004; Plotkin et al. 2012; Gültekin et al. 2019b). When restricting our analysis to only those primary sample sources with the most accurate (redshift-independent) distances, we obtain much tighter correlations (see Section 4.4), with σ_{int} comparable to that of the tightest scaling relations in astronomy (such as the Baryonic Tully–Fisher relation; e.g. Lelli, McGaugh & Schombert 2016; Lelli et al. 2019). This

technique – if sufficiently verified – is thus well-suited to constrain the details of SMBH-host galaxy co-evolution in regimes that have been difficult to access up to now (see also Williams et al. 2023).

ACKNOWLEDGEMENTS

IR and TAD acknowledge support from grant number ST/S00033X/1 through the UK Science and Technology Facilities Council (STFC). MB and TGW were supported by STFC consolidated grant ‘Astrophysics at Oxford’ ST/H002456/1 and ST/K00106X/1. DH acknowledges support from the Canada Research Chairs (CRC) programme, the NSERC Discovery Grant programme, and the Canadian Tri-Agency New Frontiers in Research – Explorations fund. This paper makes use of ALMA data. ALMA is a partnership of ESO (representing its member states), NSF (USA), and NINS (Japan), together with NRC (Canada), NSC and ASIAA (Taiwan), and KASI (Republic of Korea), in cooperation with the Republic of Chile. The Joint ALMA Observatory is operated by ESO, AUI/NRAO, and NAOJ. We acknowledge also the usage of the HyperLeda data base and the NASA/IPAC Extragalactic Database (NED).

DATA AVAILABILITY

The ALMA data used in this article are all available to download at the ALMA archive (<https://almascience.nrao.edu/asax/>). The calibrated data, final products, and original plots generated for this research study will be shared upon reasonable request to the first author. The X-ray data have been retrieved from the catalogue of Bi, Feng & Ho (2020) or from the NASA/IPAC Extragalactic Database (NED; <https://ned.ipac.caltech.edu/>).

REFERENCES

- Behar E., Vogel S., Baldi R. D., Smith K. L., Mushotzky R. F., 2018, *MNRAS*, 478, 399
- Behar E. et al., 2020, *MNRAS*, 491, 3523
- Bi S., Feng H., Ho L. C., 2020, *ApJ*, 900, 124
- Boroson B., Kim D.-W., Fabbiano G., 2011, *ApJ*, 729, 12
- Cappellari M. et al., 2013, *MNRAS*, 432, 1709
- D’Onofrio M., Marziani P., Chiosi C., 2021, *Front. Astron. Space Sci.*, 8, 157
- Davis T. A., Bureau M., Onishi K., Cappellari M., Iguchi S., Sarzi M., 2017, *MNRAS*, 468, 4675
- Davis T. A. et al., 2022, *MNRAS*, 512, 1522
- Elford J. S. et al., 2023, WISDOM Project—XVI. The link between circumnuclear molecular gas reservoirs and active galactic nucleus fuelling, Submitted to *MNRAS*
- Falcke H., Körding E., Markoff S., 2004, *A&A*, 414, 895
- Farrah D. et al., 2023, *ApJ*, 943, 133
- Fawcett V. A., Alexander D. M., Rosario D. J., Klindt L., Fotopoulou S., Lusso E., Morabito L. K., Calistro Rivera G., 2020, *MNRAS*, 494, 4802
- Fernández-Ontiveros J. A., López-Gonzaga N., Prieto M. A., Acosta-Pulido J. A., Lopez-Rodriguez E., Asmus D., Tristram K. R. W., 2019, *MNRAS*, 485, 5377
- Fernández-Ontiveros J. A., López-López X., Prieto A., 2023, *A&A*, 670, A22
- Girdhar A. et al., 2022, *MNRAS*, 512, 1608
- Grimm H. J., Gilfanov M., Sunyaev R., 2003, *MNRAS*, 339, 793
- Gültekin K. et al., 2009, *ApJ*, 698, 198
- Gültekin K., King A. L., Cackett E. M., Nyland K., Miller J. M., Di Matteo T., Markoff S., Rupen M. P., 2019a, *ApJ*, 871, 80
- Gültekin K., King A. L., Cackett E. M., Nyland K., Miller J. M., Di Matteo T., Markoff S., Rupen M. P., 2019b, *ApJ*, 871, 80
- Heckman T. M., Best P. N., 2014, *ARA&A*, 52, 589
- Ho L. C., 2008, *ARA&A*, 46, 475
- Kawamuro T. et al., 2022, *ApJ*, 938, 87

- Kim D.-W., Fabbiano G., 2004, *ApJ*, 611, 846
 Kormendy J., Ho L. C., 2013, *ARA&A*, 51, 511
 Koss M. et al., 2017, *ApJ*, 850, 74
 Koss M. J. et al., 2022, *ApJS*, 261, 2
 Lelli F., McGaugh S. S., Schombert J. M., 2016, *ApJ*, 816, L14
 Lelli F., McGaugh S. S., Schombert J. M., Desmond H., Katz H., 2019, *MNRAS*, 484, 3267
 Lucchini M. et al., 2022, *MNRAS*, 517, 5853
 Mahadevan R., 1997, *ApJ*, 477, 585
 McMullin J. P., Waters B., Schiebel D., Young W., Golap K., 2007, in Shaw R. A., Hill F., Bell D. J. eds, ASP Conf. Ser. Vol. 376, Astronomical Data Analysis Software and Systems XVI. p. 127
 Merloni A., Heinz S., di Matteo T., 2003, *MNRAS*, 345, 1057
 Narayan R., Yi I., 1995a, *ApJ*, 444, 231
 Narayan R., Yi I., 1995b, *ApJ*, 452, 710
 O’Dea C. P., Saikia D. J., 2020, *A&AR*, 29, 3
 Pesce D. W. et al., 2021, *ApJ*, 923, 260
 Plotkin R. M., Markoff S., Kelly B. C., K rding E., Anderson S. F., 2012, *MNRAS*, 419, 267
 Prieto M. A., Fern andez-Ontiveros J. A., Markoff S., Espada D., Gonz alez-Mart n O., 2016, *MNRAS*, 457, 3801
 Ricci C. et al., 2023, *ApJ*, 952, L28
 Rousseeuw P. J., 1984, *JASA*, 79, 871
 Saikia P., K rding E., Falcke H., 2015, *MNRAS*, 450, 2317
 Stalewski M., Fritz J., Baes M., Nakos T., Popovi c L.  ., 2012, *MNRAS*, 420, 2756
 Stalewski M., Ricci C., Ueda Y., Lira P., Fritz J., Baes M., 2016, *MNRAS*, 458, 2288
 Symeonidis M., 2022, *MNRAS*, 509, 3209
 van den Bosch R. C. E., 2016, *ApJ*, 831, 134
 Williams J. K., Gliozzi M., Bockwoldt K. A., Shuvo O. I., 2023, *MNRAS*, 521, 2897
 Yang G. et al., 2020, *MNRAS*, 491, 740

SUPPORTING INFORMATION

Supplementary data are available at [MNRASL](https://academic.oup.com/mnrasl/article/528/1/L76/7455681) online.

suppl_data

Please note: Oxford University Press is not responsible for the content or functionality of any supporting materials supplied by the authors. Any queries (other than missing material) should be directed to the corresponding author for the article.

This paper has been typeset from a $\text{\TeX}/\text{\LaTeX}$ file prepared by the author.